Available online at www.sciencedirect.com
ScienceDirect
Journal of Computational Physics 227 (2008) 6696–6714
JOURNAL OF COMPUTATIONAL PHYSICS
www.elsevier.com/locate/jcp

A Lagrangian, stochastic modeling framework for multi-phase flow in porous media

Manav Tyagi [a,*], Patrick Jenny [a], Ivan Lunati [b], Hamdi A. Tchelepi [c]

[a] *Institute of Fluid Dynamics, Sonnegstrasse 3, ETH Zurich, Zuerich, CH-8092, Switzerland*
[b] *Laboratory of Environmental Fluid Mechanics, GR A0 455, Station 2, Lausanne, CH-1015, Switzerland*
[c] *Department of Energy Resources Engineering, Stanford University, Stanford, CA 94305, USA*

Received 1 March 2007; received in revised form 11 March 2008; accepted 17 March 2008
Available online 1 April 2008

Abstract

Many of the complex physical processes relevant for compositional multi-phase flow in porous media are well understood at the pore-scale level. In order to study CO_2 storage in sub-surface formations, however, it is not feasible to perform simulations at these small scales directly and effective models for multi-phase flow description at Darcy scale are needed. Unfortunately, in many cases it is not clear how the micro-scale knowledge can rigorously be translated into consistent macroscopic equations. Here, we present a new methodology, which provides a link between Lagrangian statistics of phase particle evolution and Darcy scale dynamics. Unlike in finite-volume methods, the evolution of Lagrangian particles representing small fluid phase volumes is modeled. Each particle has a state vector consisting of its position, velocity, fluid phase information and possibly other properties like phase composition. While the particles are transported through the computational domain according to their individual velocities, the properties are modeled via stochastic processes honoring specified Lagrangian statistics. Note that the conditional expectations of the particle velocities are different for different fluid phases. The goal of this paper is to present the general framework for this alternative modeling approach. Various one and two-dimensional numerical experiments demonstrate that with appropriate stochastic rules the particle solutions are consistent with a standard two-phase Darcy flow formulation. In the end, we demonstrate how to model non-equilibrium phenomena within the stochastic particle framework, which will be the main focus of the future work.

Keywords: Stochastic particle method; Lagrangian approach; Porous media; Multi-phase flow; PDF method

1. Introduction

Flow and transport processes in natural porous media are usually described using differential equations defined on the macroscopic (Darcy) scale. For slow single-phase flow in a homogeneous porous medium, Darcy's law is an expression of momentum conservation at the macroscopic scale. When multiple immiscible

* Corresponding author. Tel.: +41 44 632 4505; fax: +41 44 632 1147.
E-mail address: tyagi@ifd.mavt.ethz.ch (M. Tyagi).

0021-9991/$ - see front matter © 2008 Elsevier Inc. All rights reserved.
doi:10.1016/j.jcp.2008.03.030

fluid phases are present (e.g., oil, super-critical CO_2 and water), the permeability in Darcy's original equation is replaced by an effective value to accommodate the presence of other phases in the porous medium [1]. This effective parameter is expressed as a function of phase saturation and is called relative permeability. Macroscopic capillary effects are introduced by considering different pressures in the different fluid phases. The capillary pressure relations are also usually expressed as functions of saturation.

In addition to saturation, the relative permeability and capillary pressure relations depend on the pore-scale geometry, network topology, wettability characteristics, viscosity ratio of the fluids, and saturation history. The physical interactions that take place in the rock-fluids system at the pore (microscopic) scale dictate the behavior observed at the macroscopic scale. The complexity of the small-scale dynamics has precluded the development of a general approach that links the pore-scale physics and the representation at the Darcy scale [2]. Thus, in practice the relative permeability and capillary relations, which are assumed to be appropriate macroscopic-scale descriptions, are obtained by performing laboratory flow experiments using specimens (cores) of the porous medium of interest.

This simple Darcy scale representation of the relative permeability and capillary relations is thought to be applicable for two-phase flow under strongly wetting conditions when the viscosity ratio is close to unity, and the macroscopic flow is within a relatively small range of capillary numbers [3]. In other cases of practical interest, such as EOR (enhanced oil recovery) gas injection processes and the injection and post injection periods associated with CO_2 sequestration in aquifers and reservoirs, the application of this simple model is questionable.

The mean flow velocity of reservoir displacement processes is quite small (a few centimeters per day) and the characteristic pore size of the medium is also very small. So the Reynolds number is much less than unity, and the flow at the pore scale is expected to usually be in the Stokes regime, in which the inertial effects are negligible and the pressure drop takes place entirely due to viscous and capillary forces. In these cases, the problem at the pore level is well defined and can be solved, if the pore scale geometry is known. However, even a small sample of a real porous medium contains millions of pores and in most cases it is very difficult to obtain the complete description of the pore scale geometry [4].

While the small scale flow dynamics are interesting, the objective is to construct a model based on relations that represent the macroscopic (Darcy scale and larger) behaviors accurately. The model must account for the dynamic effects of the pore scale physics on the large-scale flow. In the standard approach, the assumption is that the pore scale physics is accounted for in the relative permeability and capillary relations, which are obtained from experiments. However, this standard treatment is not well suited, if the flow involves complex processes such as non-equilibrium phenomena and residual trapping. In such flows, a statistical approach is more appropriate, since a small elemental volume of the porous media contains a large number of pores. Here we develop a statistical method for multi-phase transport in porous media using stochastic particles.

Particle tracking methods have been employed successfully in subsurface flow simulations. From the pioneering works of [5,6], fully Lagrangian schemes based on random walk approach have been widely employed for tracer (i.e. unit-viscosity, miscible, single-phase) transport. Extension of the particle-tracking approach to more complex geometry [7] and reactive flows in highly heterogeneous formations [8] appeared later. A hybrid Eulerian–Lagrangian method, where particle tracking is employed to represent the transport, was developed and used to model unstable first-contact miscible (two-component, single-phase flow) displacements in the presence of density and viscosity differences [9]. In these particle tracking methods, each particle represents a physical mass. The concentration of the tracked species (e.g. tracer) is obtained by averaging over the control volume. Relatively large particle numbers and fine grids are necessary to obtain reasonably accurate concentration distributions in the domain.

Several Eulerian–Lagrangian schemes have been introduced for linear tracer transport (see, e.g. [10–14]) and extended to nonlinear problems such as solving the saturation equation for two-phase immiscible flow (see, e.g., [15–17]). Fully Lagrangian methods have also been applied to reactive-tracer transport with nonlinear accumulation term (see, e.g., [18,19]; or [20] for a comprehensive review), which requires the calculation of concentration at the node of a superimposed grid [21]. Unlike particle tracking schemes, here concentrations are propagated along path lines. Streamline-based methods, which belong to this family, have been developed for modeling multi-component multi-phase displacement processes in heterogeneous domains [22]. Character-

istic based methods have been employed for nonlinear immiscible two-phase flow where particles are moved with the characteristic velocities and saturation is a particle property [23,24].

We developed a stochastic particle based model for nonlinear immiscible multi-phase flow, where the phase flux is a nonlinear function of saturation (e.g., as for the Buckley–Leverett problem). In our approach, a particle belongs to a specific fluid phase (e.g., water and oil particles) and moves with the phase particle velocity. The saturation is a statistical quantity defined for an ensemble of the particles. Thus, our method is different from the characteristic based methods, where particles move with the characteristic velocity and saturation is associated with the particles. In the stochastic particle method (SPM) framework, we essentially construct a model for the large scale dynamics based on stochastic rules for the phase particle behavior at the pore scale.

A similar approach was proposed in a previous, unpublished attempt [25]. It was found that, it is impossible to solve nonlinear hyperbolic problems with shocks numerically using stochastic particles. Solving a nonlinear hyperbolic problem using stochastic particles requires the estimation of ensemble averaged quantities (e.g. saturation) which implies averaging over finite volumes. For numerical reasons this does not work for discontinuous solutions and therefore, a minimum amount of diffusion (depending upon the size of averaging volume) must be introduced. Note that the size of the averaging volume determines the resolution. In the limit of infinitely many particles, the size of the averaging volume can be chosen infinitely small, which allows to solve purely hyperbolic problems. Note, however, that most macroscopic physical scenarios of interest depict diffusive effects; e.g. due to capillary pressure differences or pore scale dispersion.

Note that it is not intended to employ SPM to solve problems, which can already be computed with continuum methods. The motivation is a framework, which offers an alternative modeling approach, i.e. from a Lagrangian viewpoint. Such a Lagrangian framework is a natural way to represent non-equilibrium phenomena by specifying the physical rules governing the particle evolution at the micro-scale. Moreover, a consistent probability density function (PDF) transport equation can be formulated, which allows to derive corresponding Eulerian moment equations [26].

We demonstrate that in the limiting case of zero correlation time and length scales, the macroscopic equations derived from the microscopic model reduce to the standard Darcy scale (macroscopic) equations. In more general cases, however, additional terms and closure models are required (which requires no modeling in the stochastic particle method), if an Eulerian approach is used. There are no inherent limitations in the methodology, provided the required Lagrangian statistics can be specified, e.g. from experiments or pore network simulations. Such a consistent multi-scale multi-physics framework allows for more insight into the physics governing multi-phase flow in natural porous media; moreover, this framework can help in deriving effective coefficients and proposing modified macroscopic models.

2. Basic ideas

In this section, we explain the basic ideas of the stochastic particle method (SPM). Therefore, the nonlinear transport problem

$$\frac{\partial \rho_i}{\partial t} + \nabla \cdot \boldsymbol{F}_i = q_i \quad \text{for } i \in \{1, \ldots, n\} \text{ on } \Omega \tag{1}$$

with some boundary conditions at $\partial\Omega$ is considered, where ρ_i, $\boldsymbol{F}_i$ and q_i are the density of a conserved scalar, flux vector and rate of production, respectively. Now, we consider a large number of computational particles, each associated with one of the n scalars. Here, the density $\rho_i = w_i \rho_i^{pn}$ represents the concentration of i-particles, where w_i is the particle weight and ρ_i^{pn} the particle number density. Next, it is shown how to evolve the particles in order to compute the solution of Eq. (1). By integrating Eq. (1) over a control volume $\Omega' \subset \Omega$ one obtains

$$\int_{\Omega'} \frac{\partial \rho_i}{\partial t} \mathrm{d}\Omega + \int_{\Omega'} \nabla \cdot \boldsymbol{F}_i \, \mathrm{d}\Omega = \int_{\Omega'} q_i \, \mathrm{d}\Omega \quad \text{for } i \in \{1, \ldots, n\}. \tag{2}$$

Using Gauss' theorem and with the relation $\rho_i = w_i \rho_i^{pn}$ one obtains the equivalent expression

$$\frac{\partial}{\partial t} \underbrace{\int_{\Omega'} \rho_i^{pn} \, \mathrm{d}\Omega}_{n_i^{\Omega'}} = - \int_{\partial\Omega'} \underbrace{\frac{\boldsymbol{F}_i}{w_i} \cdot \boldsymbol{v} \, \mathrm{d}\Gamma}_{\mathrm{d}\mathcal{F}_i} + \int_{\Omega'} \frac{q_i}{w_i} \mathrm{d}\Omega \quad \text{for } i \in \{1, \ldots, n\}, \tag{3}$$

where $\boldsymbol{v}$ is the unit normal vector at $\partial\Omega'$ pointing outwards. The first term in Eq. (3) is the rate at which the number $n_i^{\Omega'}$ of i-particles in Ω' changes. The first right-hand side term describes the contribution due to particle fluxes across the boundary $\partial\Omega'$, which has to balance the left-hand side term and the last term on the right-hand side (rate at which particles are created inside Ω'). Now, we show that the evolution of the particle concentration ρ_i is consistent with Eq. (1), if the i-particles are transported with the velocity

$$\boldsymbol{u}_i^* = \frac{\boldsymbol{F}_i}{\rho_i} = \frac{\boldsymbol{F}_i}{w_i \rho_i^{pn}}. \tag{4}$$

The superscript $*$ denotes that a quantity is a particle property. While $\boldsymbol{u}_i^*$ is the velocity of an individual particle, ρ_i^{pn} is the particle number density in its neighborhood. Note that we assume to know both $\boldsymbol{F}_i$ and ρ_i at the particle locations. The rate of particles flowing across a surface element $\mathrm{d}\Gamma$ is

$$\rho_i^{pn} \boldsymbol{u}_i^* \cdot \boldsymbol{v} \, \mathrm{d}\Gamma = \rho_i^{pn} \frac{\boldsymbol{F}_i}{\rho_i} \cdot \boldsymbol{v} \, \mathrm{d}\Gamma = \frac{\boldsymbol{F}_i}{w_i} \cdot \boldsymbol{v} \, \mathrm{d}\Gamma, \tag{5}$$

which is identical to $\mathrm{d}\mathcal{F}_i$ in Eq. (3). Thus, we have shown that Eq. (2) is solved consistently, if the particles are evolved according to Eq. (4). Moreover, since this is true for any arbitrary volume $\Omega' \subset \Omega$, the particle solution converges to the exact solution of Eq. (1) for $|\Omega'| \to 0$ and an infinite number of particles.

3. Model for multi-phase flow in porous media

In this section, it is shown how the SPM introduced in the previous section can be employed to solve for multi-phase transport in porous media. We consider n phases, each represented by a number of computational particles. All particles of phase i have the same mathematical weight $w_i = V_i$, where V_i is the volume occupied by a particle. One could also choose w_i being proportional to the mass associated to a particle and the volume being a function of pressure and weight. For incompressible fluid it is easier, however, to directly take the particle weight to be equal to the volume. In an arbitrary volume $\Omega' \subset \Omega$, the number of phase i particles is equal to

$$n_i^{\Omega'} = \int_{\Omega'} \rho_i^{pn} \, \mathrm{d}\Omega = \int_{\Omega'} \frac{\rho_i}{V_i} \mathrm{d}\Omega, \tag{6}$$

where $\int_{\Omega'} \rho_i \, \mathrm{d}\Omega$ is the volume represented by these particles. The accessible pore space inside Ω' is $\int_{\Omega'} \phi \, \mathrm{d}\Omega$, where the porosity is defined as $\phi = \sum_{j=1}^{n} \rho_j$. The phase saturations

$$S_i = \frac{\rho_i}{\phi} = \frac{V_i \rho_i^{pn}}{\phi} \tag{7}$$

are proportional to the particle number density. Assuming that the fluids and the rock are incompressible ($V_i = \text{constant}$ and $\phi = \phi(\boldsymbol{x})$) we can write the saturation equations as

$$\phi \frac{\partial S_i}{\partial t} + \nabla \cdot \boldsymbol{F}_i = q_i, \quad i \in \{1, \ldots, n\}, \tag{8}$$

which is consistent with Eq. (1). In accordance with Eq. (4), each particle moves with velocity

$$\boldsymbol{u}_i^* = \frac{\boldsymbol{F}_i}{\phi S_i}. \tag{9}$$

It should be noted that at this point the source terms q_i represent only well rates and are explicitly specified. These source terms can easily be treated in the SPM framework. Each particle represents either mass or volume of the fluid phase to which it belongs. Therefore, to be consistent with the source term at some location in the domain, particles might be removed or additional particles are introduced; according to the local mass flow rate. Summing Eq. (8) over all phases and using the fact that $\sum_{j=1}^{n} S_j \equiv 1$ we obtain

$$\nabla \cdot \overbrace{\sum_{j=1}^{n} \boldsymbol{F}_j}^{\boldsymbol{F}} = \overbrace{\sum_{j=1}^{n} q_j}^{q}. \tag{10}$$

In the absence of sources and sinks, the total flux $\boldsymbol{F}$ is divergence free.

So far, we have derived a discrete representation that is consistent with the continuum Eq. (8), where phase particles move with the velocity given by Eq. (9). Here, for illustration purpose, it is assumed that the large scale (Darcy scale) fluxes $\boldsymbol{F}_i$ are governed by Darcy's law and read

$$\boldsymbol{F}_i = -\frac{k_{r_i} k}{\mu_i} \nabla p_i, \quad i \in \{1, \ldots, n\}, \tag{11}$$

where k is the rock permeability and k_{r_i}, μ_i and p_i are the relative permeability, viscosity and pressure of phase i, respectively. Usually, empirical expressions are used to relate k_{r_i} and $p_{c_{i-1}} = p_{i-1} - p_i$ with the phase saturations. Substituting the fluxes (11) into Eq. (10) leads to the following elliptic equation

$$\nabla \cdot \overbrace{\left(-\sum_{j=1}^{n} \frac{k_{r_j} k}{\mu_j} \nabla p_j \right)}^{\boldsymbol{F}} = q. \tag{12}$$

In Appendix, we show how Eq. (11) can be rewritten in the following fractional flow formulation

$$\boldsymbol{F}_i = \frac{\lambda_i}{\lambda} \boldsymbol{F} + \frac{-(\lambda_i k) \sum_{l=1}^{n} (\lambda_l \sum_{j=1}^{l-1} \nabla p_{cj}) + \lambda_i k \lambda \sum_{j=1}^{i-1} \nabla p_{cj}}{\lambda}, \quad i \in \{1, \ldots, n\}, \tag{13}$$

where $\lambda_i = k_{r_i}/\mu_i$ are the phase mobilities and $\lambda = \sum_{j=1}^{n} \lambda_j$ the total mobility. In the general case, λ_i are functions of saturations, and therefore, the elliptic pressure equation (see Appendix for the derivation)

$$-\nabla \cdot (\lambda k \nabla p_1) + \nabla \cdot \left(k \sum_{l=1}^{n} \left(\lambda_l \sum_{j=1}^{l-1} \nabla p_{cj} \right) \right) = q \tag{14}$$

is coupled with the phase transport equations (8). One possible way to solve the system of equations is to compute the pressure field at the beginning of each time step by solving Eq. (14) and subsequent solution of the transport equations

$$\phi \frac{\partial S_i}{\partial t} + \nabla \cdot \boldsymbol{F}_i = q_i, \quad i \in \{1, \ldots, n\}. \tag{15}$$

In general, the phase fluxes $\boldsymbol{F}_i$ are functions of saturations and their gradients. Therefore, in order to compute the velocity (9) of a particle, the saturations, i.e. the phase particle number densities ρ_i^{pn}, have to be estimated in its neighborhood. For smooth saturation distributions this can be achieved by averaging over an ensemble around the particle location $\boldsymbol{x}$ and since for an infinite number of particles the volume containing that ensemble can be chosen infinitely small, this local spatial averaging procedure becomes identical with ensemble averaging at the location $\boldsymbol{x}$. If one insists in computing very sharp saturation fronts, then the averaging volume has to be extremely small and a huge number of particles have to employed. However, in a numerical simulation with a finite size averaging volume, one has to ensure that the particle distribution is nearly uniform over the averaging volume such that ergodicity can be assumed, which allows to replace ensemble by spatial averaging. Below we discuss two ways how this can be achieved.

3.1. Random walk method

In real porous media flows there are various pore scale phenomena that result in dispersive effects at the continuum scales, e.g. due to capillary pressure differences, molecular diffusion and mechanical dispersion. Therefore, there exist no infinitely sharp fronts at the macroscale. Mechanical dispersion can be treated adequately by adding a diffusion term to Eq. (8), which leads to the modified saturation equation

$$\phi \frac{\partial S_i}{\partial t} + \nabla \cdot \boldsymbol{F}_i = \nabla \cdot D \nabla S_i + q_i, \quad i \in \{1, \ldots, n\}. \tag{16}$$

Note that in general D is not constant in space and depends on $|\boldsymbol{F}_i|$ and on the saturation. To compute a numerical solution in the presence of these dispersive phenomena we only need to resolve the smallest length scale l that captures the corresponding effects at the continuum scales. In practice, therefore, the characteristic size of the averaging volume must be in the neighborhood of l. A particle evolution in physical space, which is consistent with Eq. (16), is given by

$$d\boldsymbol{x}_i^* = \boldsymbol{u}_i^* \, \mathrm{d}t = \frac{\boldsymbol{F}_i}{\phi S_i} \mathrm{d}t + \sqrt{\frac{2D}{\phi}} \mathrm{d}\boldsymbol{W} + \frac{1}{\phi} \nabla D \, \mathrm{d}t, \tag{17}$$

where $\boldsymbol{F}_i$ is given by Eq. (13). Note that $\boldsymbol{F}_i$ also include diffusive fluxes due to capillary pressure differences. The second right-hand side term of Eq. (17) is a Wiener process, where each component of $\mathrm{d}\boldsymbol{W} = (\mathrm{d}W_1, \mathrm{d}W_2, \mathrm{d}W_3)^{\mathrm{T}}$ has a Gaussian distribution with $\langle \mathrm{d}W_k \rangle \equiv 0$ and $\langle \mathrm{d}W_k \, \mathrm{d}W_l \rangle = \delta_{kl} \, \mathrm{d}t$. The last term is necessary to account for spatially varying coefficient D. One should remember that Eq. (17) does not account for the source term in Eq. (16). As mentioned before, in order to account for the source term, particles have to be introduced or destroyed at consistent rates. In our simulations, this is necessary in grid cells, which are perforated by a well.

3.2. Shaking method

If one is not interested in resolving the length scales associated with physical diffusion, an alternative approach can be used. First particles are moved with the velocity given by Eq. (9). After each time step one assigns arbitrary new particle positions within the same cell. Computationally, this can be done by uniformly redistributing ("shaking") the particles in a cell after each time step. With a uniform distribution of particles in a cell, local ergodicity can be assumed, i.e. the particles in a cell represent the distribution at one point in space and time. Important is that thereby the other particle properties are not affected, such that the particle properties of the ensemble still exhibit the same distribution. Note, however, that the resulting diffusion is dictated by the grid and cannot directly be controlled.

4. Solution algorithm

We solve the flow equation (14) for pressure using a finite-volume method (FVM). The macroscopic transport Eq. (16), on the other hand, is solved with the SPM, which is fully Lagrangian method, where the particle evolution is given by Eq. (17). To solve the transport equation, the whole domain is populated with various phase particles (consistent with the initial condition). The following quantities are needed to evolve the particles: $\boldsymbol{F}$, S_i, ∇p_c and ∇D. Since these quantities are only available at the grid level, they have to be interpolated to the particle locations. In order to ensure mass balance, linear interpolation of $\boldsymbol{F}$ from the cell faces to the particle locations is used. To estimate S_i, simple cell averaging is employed at this point. The evolution of an individual particle is computed with a second or fourth order Runge–Kutta scheme. For example, in the second order scheme a particle is first transported according to

$$\boldsymbol{x}^{*^{n+1/2}} = \boldsymbol{x}^{*^n} + \left(\frac{\boldsymbol{F}_i}{\phi S_i} + \frac{1}{\phi} \nabla D \right) \frac{\mathrm{d}t}{2}. \tag{18}$$

All terms in the brackets are evaluated at location $\boldsymbol{x}^{*^n}$. Finally, the new particle position is obtained through

$$\boldsymbol{x}^{*^{n+1}} = \boldsymbol{x}^{*^n} + \left(\frac{\boldsymbol{F}_i}{\phi S_i} + \frac{1}{\phi} \nabla D \right) \mathrm{d}t + \sqrt{\frac{2D \, \mathrm{d}t}{\phi}} \boldsymbol{\xi}, \tag{19}$$

where the total flux $\boldsymbol{F}$ is evaluated at $\boldsymbol{x}^{*^{n+1/2}}$ and all other quantities at $\boldsymbol{x}^{*^n}$. Note that the components of the vector $\boldsymbol{\xi} = (\xi_1, \xi_2, \xi_3)^{\mathrm{T}}$ are independent random variables with standard Gaussian distribution. It should be mentioned that in the above scheme, higher order accuracy is obtained only if S_i and D in Eq. (19) are

evaluated at the mid point $\boldsymbol{x}^{*^{n+1/2}}$. A more detailed discussion on higher order integration of stochastic differential equations can be found in [27]. Initially, the particles are distributed according to the specified saturation distribution. At the beginning of each time step, $\boldsymbol{F}$ is computed by the FVM and subsequently the particles are transported as described above. In order to deal with in- and out-flow boundary conditions, the computational domain is surrounded with a layer of ghost cells, which can be re-populated consistently with the specified boundary conditions at the beginning of each time step [28]. Re-population is also applied in cells where a source is employed (wells). No-flow boundaries are treated by simply reflecting the particles at the corresponding walls.

5. Numerical validation

In this section we demonstrate that the SPM is consistent with the governing equations. In order to show convergence, the SPM results are compared with corresponding FVM reference solutions (using up to ten times finer grids to avoid numerical dispersion). For all the results presented here two phases ($n = 2$) with the flux functions

$$\boldsymbol{F}_1 = \frac{\lambda_1}{\lambda}\boldsymbol{F} - \frac{k\lambda_1\lambda_2}{\lambda}\nabla p_c \quad \text{and} \quad \boldsymbol{F}_2 = \frac{\lambda_2}{\lambda}\boldsymbol{F} + \frac{k\lambda_1\lambda_2}{\lambda}\nabla p_c \tag{20}$$

are considered, where

$$p_c = p_1 - p_2 \tag{21}$$

is the capillary pressure difference between the two phases. We take the quadratic relative permeabilities functions as

$$\lambda_1 = \frac{S^2}{\mu_1} \quad \text{and} \quad \lambda_2 = \frac{(1-S)^2}{M\mu_1}, \tag{22}$$

where $M = \mu_2/\mu_1$ is the viscosity ratio. The saturations of phase one and phase two are $S_1 = S$ and $S_2 = 1 - S$, respectively. To treat stochastic component of diffusion we employ random walk method. Note that all quantities are presented in dimensionless form.

5.1. 1D validation

For initial validation purpose, a simple 1D problem is considered. In the following results, the dimensionless space and time coordinates $\boldsymbol{x}' = \boldsymbol{x}/L$ and $t' = Ft/(\phi L)$ are used. At time $t' = 0$, the saturation $S_1 = S$ is one in the whole reservoir. Then, for $t' > 0$, phase two is injected at the left boundary ($S_2 = 1 - S = 1$ at $x' = 0$). The total volume flux F is constant during the whole simulation. For the first studies, no capillary pressure effect is considered, i.e. $p_c = 0$, and the diffusion coefficient D is chosen such that the grid Peclet number

$$Pe = \frac{F\Delta x}{D} \tag{23}$$

is one, where Δx is the grid spacing used for the SPM. Note that the SPM requires a grid Peclet number, which is not much larger than one. Figs. 1 (a) and (b) show the saturation profiles of phase two for $M = 1$ after the time $t' = 0.25$ obtained with the grid spacings $\Delta x' = 0.01$ and 0.002, respectively and $Pe = 1$. The good agreement between the SPM (solid lines) and FVM (dotted lines) solutions demonstrates that the two methods are consistent. Note that the grid spacing used for the FVM is $\Delta x'/10$ in order to provide a good reference. In order to keep the statistical error of the SPM results very small, a huge number of particles, i.e. on average 50,000 per grid cell, were employed. Note, however, that the SPM also works with much fewer particles. Fig. 2 shows SPM and FVM results for various viscosity ratios M and a grid spacing $\Delta x' = 0.01$ (0.001 for the FVM).

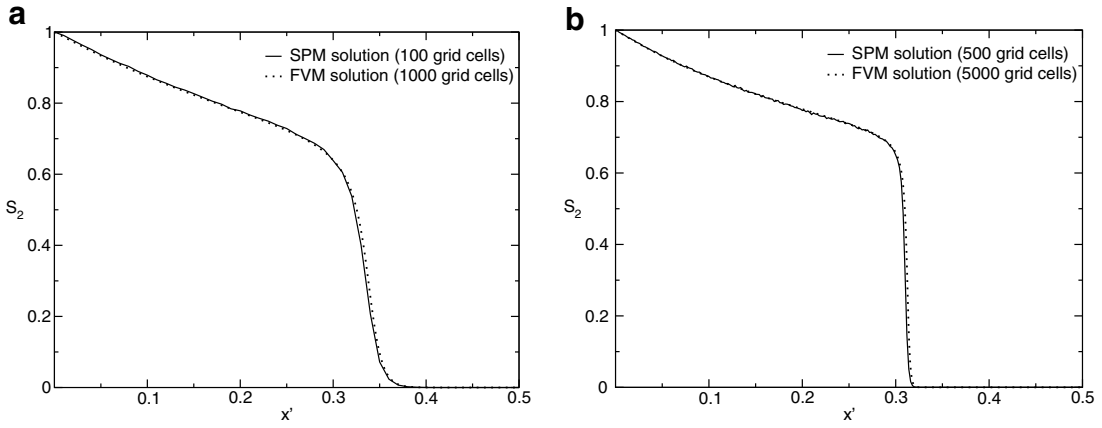

Fig. 1. Simulation results of the 1D test case for $M = 1$: (a) $\Delta x' = 0.01$; (b) $\Delta x' = 0.002$.

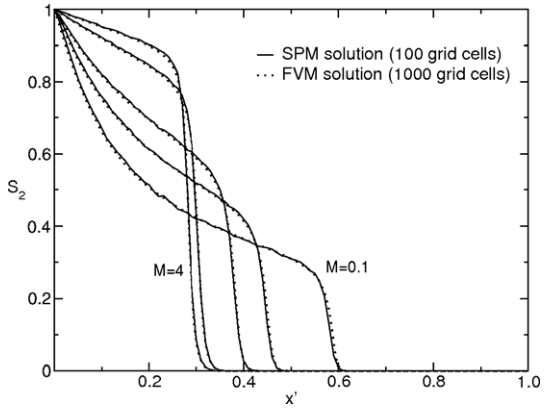

Fig. 2. Simulation results of the 1D test case for different values of $M = 4, 2, 0.5, 0.25, 0.1$ and $\Delta x' = 0.01$.

Next, we consider the same 1D problem with capillary pressure, i.e. with

$$p_c = \begin{cases} -p_0/S & \text{for drainage} \\ p_0/(1-S) & \text{for imbibition.} \end{cases} \tag{24}$$

Substituting Eqs. (22) and (24) into Eq. (20) leads to the flux functions

$$\boldsymbol{F}_1 = \frac{MS^2}{MS^2 + (1-S)^2}\boldsymbol{F} - C\nabla S \quad \text{and} \tag{25}$$

$$\boldsymbol{F}_2 = \frac{(1-S)^2}{MS^2 + (1-S)^2}\boldsymbol{F} + C\nabla S \tag{26}$$

with

$$C = \begin{cases} C_0 \frac{(1-S)^2}{MS^2+(1-S)^2} & \text{for drainage} \\ C_0 \frac{S^2}{MS^2+(1-S)^2} & \text{for imbibition} \end{cases} \tag{27}$$

and $C_0 = p_0 k/\mu_1$. The corresponding dimensionless numbers are $C' = C/(FL)$ and $C'_0 = p_0 k/(\mu_1 FL)$. Note that the presence of capillary pressure leads to a saturation dependent diffusion coefficient C. Therefore, the SPM can be employed for $Pe \gg 1$, if the capillarity effects are significant. It has to be mentioned, however, that a minimum amount of randomness is required, i.e. D must not be zero. Due to technical reasons, during the initial period from $t' = 0$ to $t' = 0.05\ Pe$ and C were set to 1 and 0, respectively. For $t' > 0.05$, Pe was increased

by a factor of 10 and C was finite. Figs. 3 (a) and (b) show the saturation profiles at $t' = 0.25$ for $C' = 0.01$ and $C' = 0.02$, respectively. In all cases, the grid spacings for the SPM and the FVM are 0.01 and 0.001, respectively. It can be seen that the SPM (solid lines) and FVM (dotted lines) results are in excellent agreement. Figs. 4 (a) and (b) depict the corresponding results for imbibition.

5.2. 2D validation

The 1D validation studies show that the SPM is consistent with the FVM and that the results converge to the correct solutions. Here, it is demonstrated that the method can also be applied for multi-dimensional problems. We consider a quadratic 2D domain (quarter-five-spot configuration) Ω of size $L \times L$ with impermeable walls (Fig. 5). A source and a sink are distributed over square sub-domains as

$$q = \begin{cases} \frac{100}{L^2} q_0, & \text{if } (0 \leqslant x/L \leqslant 0.1) \wedge (0 \leqslant y/L \leqslant 0.1) \\ -\frac{100}{L^2} q_0, & \text{if } (0.9 \leqslant x/L \leqslant 1) \wedge (0.9 \leqslant y/L \leqslant 1) \\ 0, & \text{else,} \end{cases} \tag{28}$$

where phase two is injected at the lower left corner (the viscosity ratio M is one in all cases). Initial conditions at $t = 0$ are

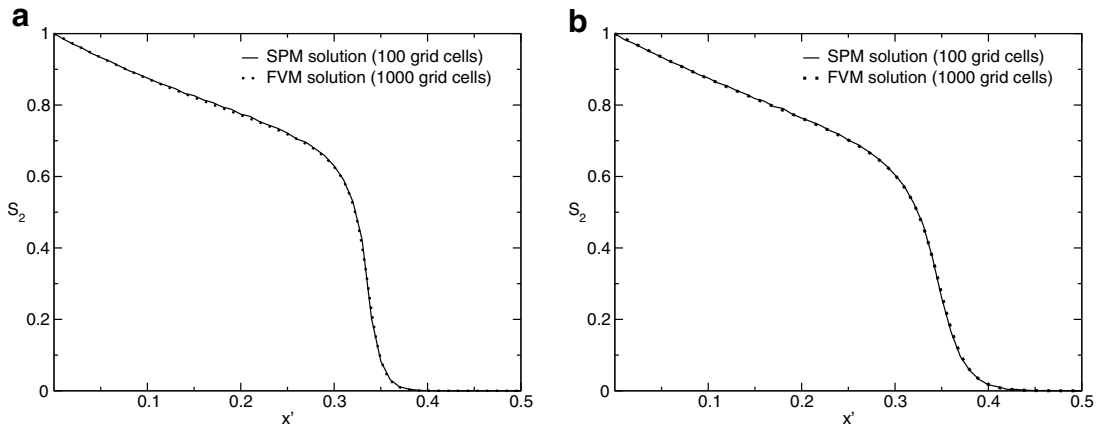

Fig. 3. Simulation results with $M = 1$ and a constant diffusion coefficient: (a) $C' = 0.01$; (b) $C' = 0.02$.

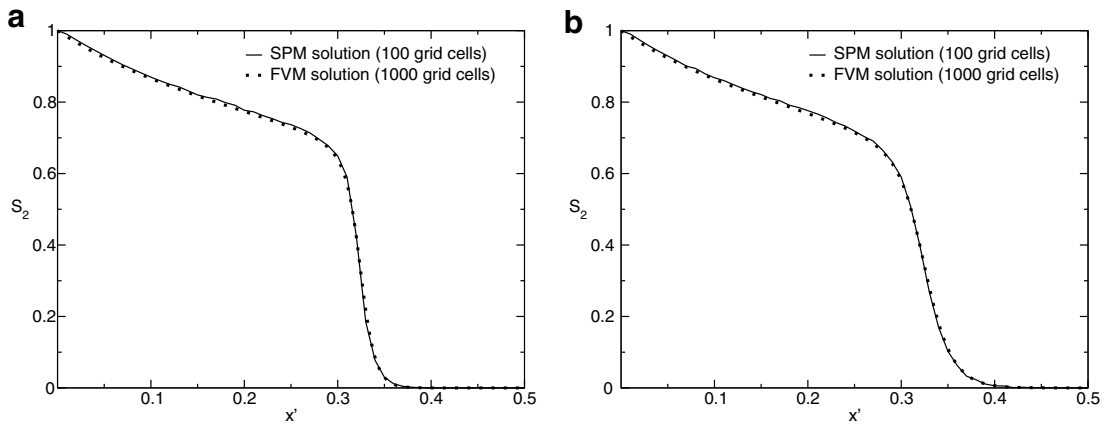

Fig. 4. Simulation results with $M = 1$ for imbibition: (a) $C'_0 = 0.01$; (b) $C'_0 = 0.02$.

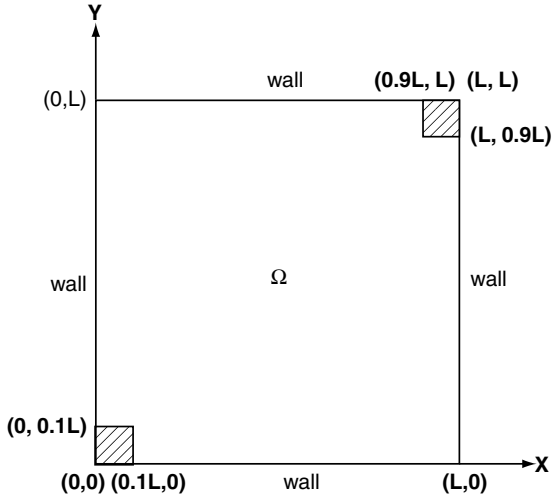

Fig. 5. Quarter-five-spot configuration. The shaded regions represent the distributed source (left-bottom corner) and sink (top-right corner).

$$S_2 = \begin{cases} 1, & \text{if } (0 \leqslant x/L \leqslant 0.11) \wedge (0 \leqslant y/L \leqslant 0.11) \\ 0, & \text{else.} \end{cases} \tag{29}$$

The domain is discretized by an orthogonal grid into 100×100 cells of equal size and for all the following results the dimensionless space and time coordinates $\boldsymbol{x}' = \boldsymbol{x}/L$ and $t' = q_0 t/(\phi L^2)$ are used. With the following studies we want to demonstrate that the SPM for transport gives consistent results. Although it is possible to update the flow field every time step, here the focus is on the transport part and the flow was computed only at the beginning of the simulations. For all the following studies an average number of 16,000 particles per cell and a fourth order particle tracking scheme were employed. Moreover, for validation purpose the SPM results are compared with the corresponding FVM solutions, for which a QUICK scheme [29] was used.

5.2.1. Homogeneous case

First, in order to demonstrate that the SPM can be applied for non-uniform multi-dimensional simulations, a homogeneous permeability field is considered. No capillary pressure effects are taken into account ($C = 0$) and dispersion is purely mechanical with $D = 0.01L|\boldsymbol{F}|$. This corresponds to a grid Peclet number of one everywhere

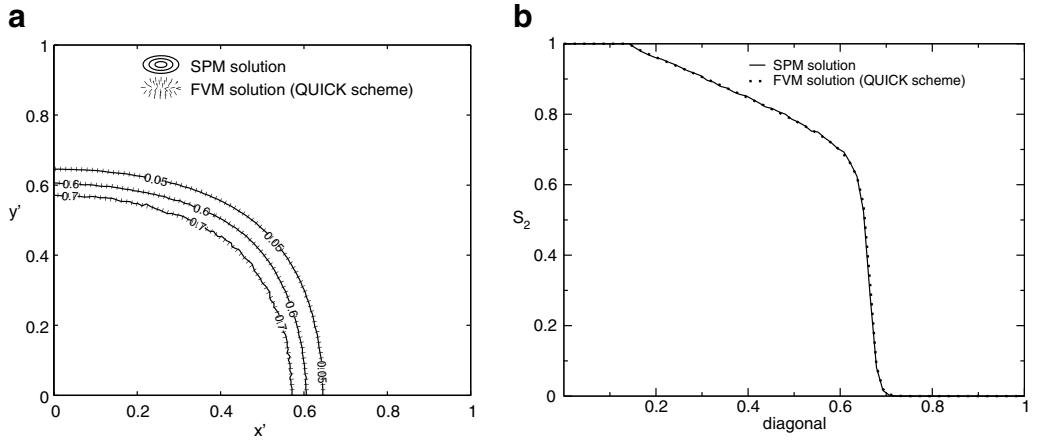

Fig. 6. Simulation results for quarter-five spot case in homogeneous permeability field and $M = 1$: (a) contours of injected phase saturation; (b) variation of injected phase saturation along the diagonal.

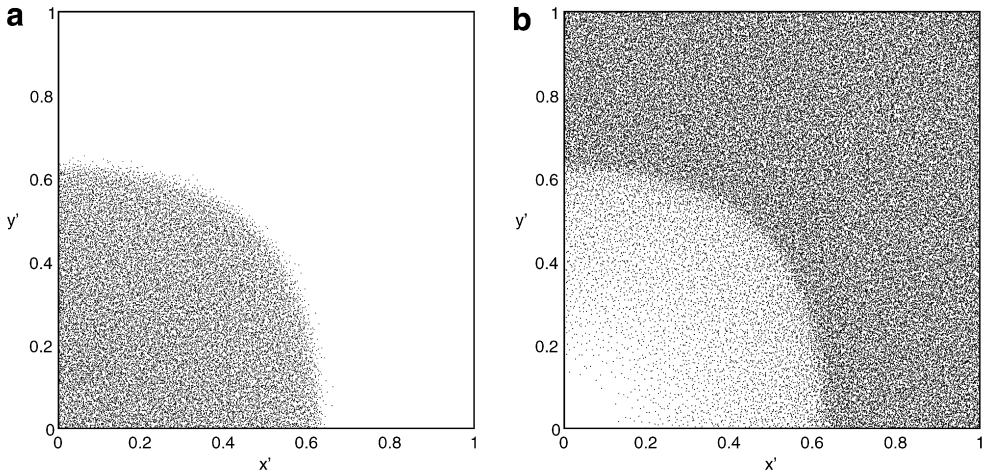

Fig. 7. Particle distributions in homogeneous permeability field and $M = 1$: (a) phase-2; (b) phase-1.

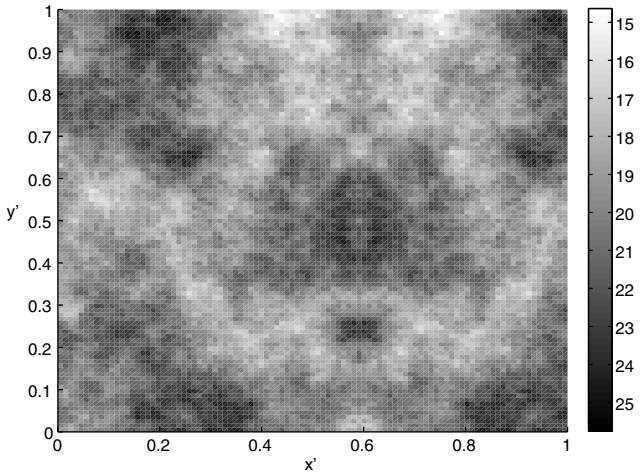

Fig. 8. Permeability field for heterogeneous test case ($\log k$).

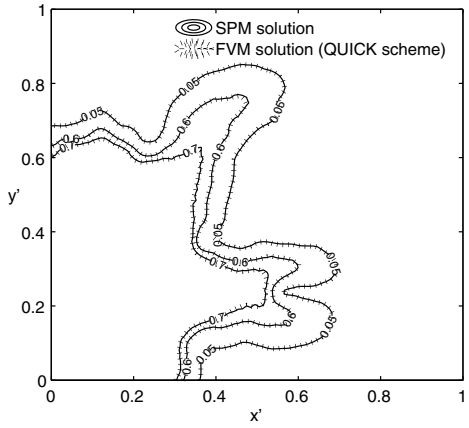

Fig. 9. Simulation results for quarter-five spot case with heterogeneous permeability field and $M = 1$; shown are contours of the injected phase saturation.

in the domain. The time step, $\Delta t'$, was equal to 0.001 corresponding to a maximum CFL number of approximately 0.5. Fig. 6 (a) depicts contours and Fig. 6 (b) profiles (along the diagonal from injector to producer) of S_2 at $t' = 0.25$. Shown are both, SPM and FVM results and as can be observed they are in excellent agreement. In addition, scatter plots of the phase two and phase one particles are shown in Fig. 7 (a) and (b), respectively. It should be noted that the sparsely distributed particles in Fig. 7 (b) represent the expansion wave and are not due to diffusive effects.

5.2.2. Heterogeneous case

Here, a more realistic case with the heterogeneous permeability field depicted in Fig. 8 ($\log k$) is considered. As in the previous study, dispersion is solely due to mechanical dispersion, i.e. $C = 0$ and $D = 0.01L|\boldsymbol{F}|$. Since the velocity variation is larger this time, $\Delta t'$ was 0.0001 to ensure a CFL number smaller than one everywhere. Again, excellent agreement between SPM and FVM results can be observed in Fig. 9, where the contours of S_2 are shown. The phase particle distributions are depicted in Fig. 10 (a) and (b).

5.2.3. Homogeneous case with capillary pressure effects

Finally, convergence is demonstrated for a 2D case with capillary pressure effects using the values 0.01 and $0.001L|\boldsymbol{F}|$ for $C'(= C/q_0)$ and D, respectively. Without loss of generality a homogeneous permeability field was

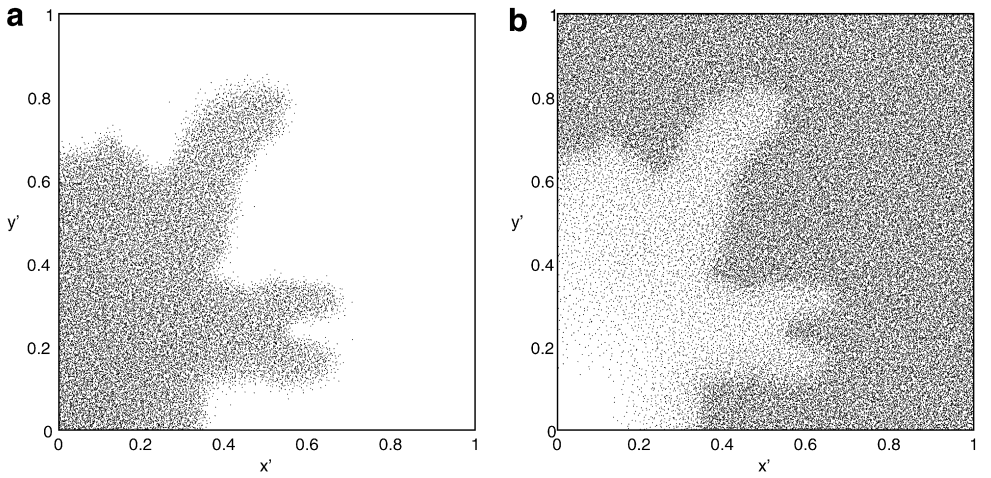

Fig. 10. Particle distribution in heterogeneous permeability field for $M = 1$: (a) phase-2; (b) phase-1.

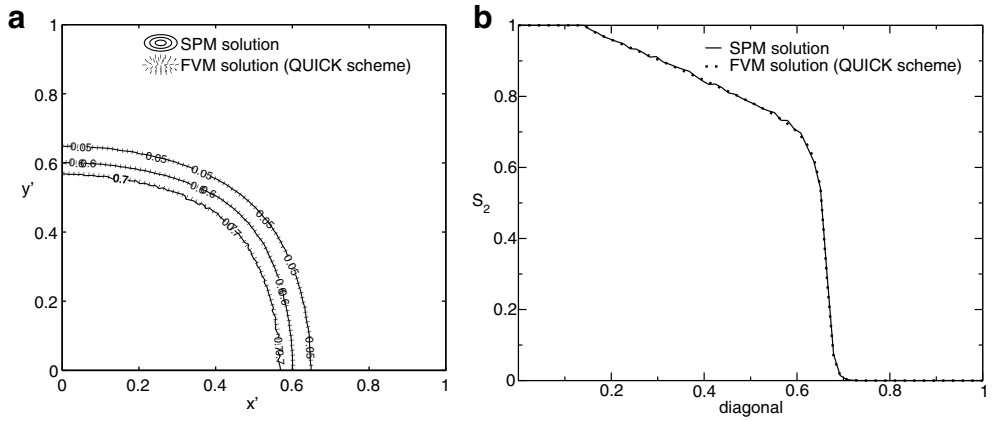

Fig. 11. Simulation results for quarter-five spot case with homogeneous permeability field, capillary pressure ($C' = 0.01$) and $M = 1$: (a) contours of injected phase saturation; (b) variation of injected phase saturation along the diagonal.

used for this study. Fig. 11 (a) depicts contours and Fig. 11 b diagonal profiles of S_2. As in the previous 2D test cases, the agreement between the SPM and FVM solutions is excellent.

6. Probability density function (PDF) modeling of non-equilibrium multi-phase systems

In this section, we demonstrate how the SPM framework can be used to derive macroscopic behavior from simple statistical rules describing the evolution of particle properties. Note that the aim is not to propose a new physical model; the scenario described next is of illustrative nature only. We consider an incompressible 1D system, initially occupied by phase one, where phase two particles are entering the domain at the left boundary. The condition at the left boundary is specified as constant total flux $F = 1$, so that the velocity of each particle entering through the left boundary is $u^* = 1$. We impose the rule that a particle representing phase $\alpha \in \{1, 2\}$ moves with the velocity

$$u^* = -L^* \frac{\partial p}{\partial x}(x^*, t), \tag{30}$$

where $\partial p/\partial x$ is the macroscopic pressure gradient and L^* a particle mobility. In other words, if L^* is one, the particle moves with the velocity $u^* = -\partial p/\partial x$ according to Darcy's law for one-phase flow and $L^* = 0$ means that the particle is immobile. The mean conditional particle velocity $\langle u^*|a^* = \alpha\rangle$ is equal to $-\langle L^*|a^* = \alpha\rangle \partial p/\partial x$, where the property $a^* = \alpha$ indicates the phase represented by the particle. By multiplying the conditional particle velocities with the corresponding saturations S_α, which can be regarded as particle number densities, we get the particle mass fluxes

$$F_1 = -S_1 \langle L^*|a^* = 1\rangle \frac{\partial p}{\partial x} \quad \text{and} \quad F_2 = -S_2 \langle L^*|a^* = 2\rangle \frac{\partial p}{\partial x}. \tag{31}$$

Due to continuity and the imposed inflow conditions at the left boundary one obtains the relation

$$F_1 + F_2 = 1. \tag{32}$$

By substituting for the pressure gradient in Eq. (30) using the relations (31), one gets the following expression for the particle velocity:

$$u^* = \frac{L^*}{S_1 \langle L^*|a^* = 1\rangle + S_2 \langle L^*|a^* = 2\rangle} \tag{33}$$

and the particle mass fluxes can be expressed as

$$F_1 = \frac{S_1 \langle L^*|a^* = 1\rangle}{S_1 \langle L^*|a^* = 1\rangle + S_2 \langle L^*|a^* = 2\rangle}$$

and

$$F_2 = \frac{S_2 \langle L^*|a^* = 2\rangle}{S_1 \langle L^*|a^* = 1\rangle + S_2 \langle L^*|a^* = 2\rangle}. \tag{34}$$

If the specific rule

$$L^* = \begin{cases} 1, & \text{with the probability } S_\alpha(x^*, t) \\ 0, & \text{else} \end{cases} \tag{35}$$

is employed, $\langle L^*|a^* = \alpha\rangle$ becomes equal S_α and as a result Eqs. (33) and (34) can be rewritten as

$$u^* = \frac{L^*}{S_1^2 + S_2^2}, \quad F_1 = \frac{S_1^2}{S_1^2 + S_2^2} \quad \text{and} \quad F_2 = \frac{S_2^2}{S_1^2 + S_2^2}, \tag{36}$$

which leads to the conservation law

$$\frac{\partial S_\alpha}{\partial t} + \frac{\partial}{\partial x}\left\{\frac{S_\alpha^2}{S_1^2 + S_2^2}\right\} = 0 \tag{37}$$

for S_α. Note that Eq. (37) is identical with the standard two-phase Darcy formulation of incompressible flow with quadratic relative permeabilities, constant viscosities, unit porosity and without capillary pressure or pore scale dispersion. In this simple case of a system in equilibrium, the conditional expectation $\langle L^*|a^*=\alpha\rangle$ is equal to S_α independent of the particle property PDF and one can also write

$$u^* = \frac{S_\alpha}{S_1^2 + S_2^2} \tag{38}$$

for the phase α particle velocities directly in terms of the saturation values and obtains the same macroscopic solutions.

Next, we introduce non-equilibrium effects by considering the Langevin model

$$\mathrm{d}L^* = -\omega_\alpha\left(L^* - \overline{L}_\alpha\right)\mathrm{d}t + \sqrt{2\sigma_\alpha^2\omega_\alpha}\,\mathrm{d}W \tag{39}$$

for the evolution of L^* of α phase particles. The first term on the right-hand side describes the relaxation of L^* to some equilibrium value $\overline{L}_\alpha$ at the rate ω_α. The last term is a stochastic diffusion term with the Wiener process $\mathrm{d}W$, which follows a Gaussian distribution with $\langle \mathrm{d}W\rangle = 0$ and $\langle \mathrm{d}W^2\rangle = \mathrm{d}t$. Note that the diffusion coefficient depends on the equilibrium variance σ_α^2 and on the rate ω_α. The stochastic differential equation (39) is constructed such that for constant coefficients L^* reaches a Gaussian equilibrium distribution with $\langle L^*|a^*=\alpha\rangle = \overline{L}_\alpha$ and $\langle (L^* - \langle L^*|a^*=\alpha\rangle)^2|a^*=\alpha\rangle = \sigma_\alpha^2$.

Now we write the general form of the joint probability density function (JPDF) evolution equation, i.e.

$$\frac{\partial f}{\partial t} + \frac{\partial\langle\frac{\mathrm{d}X}{\mathrm{d}t}|\hat{a},\widehat{L};x,t\rangle f}{\partial x} + \frac{\partial\langle\frac{\mathrm{d}a}{\mathrm{d}t}|\hat{a},\widehat{L};x,t\rangle f}{\partial \hat{a}} + \frac{\partial\langle\frac{\mathrm{d}L}{\mathrm{d}t}|\hat{a},\widehat{L};x,t\rangle f}{\partial \widehat{L}} = 0, \tag{40}$$

which can be derived from the conservation law for the joint probability density f of the stochastic variables a and L. Note that $\hat{a}$ and $\widehat{L}$ are the corresponding sample space coordinates, respectively. In our specific model, the JPDF is transported with the velocities

$$\left\langle \frac{\mathrm{d}X}{\mathrm{d}t}|\hat{a},\widehat{L};x,t\right\rangle = \frac{\widehat{L}}{S_1\langle L|\hat{a}=1\rangle + S_2\langle L|\hat{a}=2\rangle}, \tag{41}$$

$$\left\langle \frac{\mathrm{d}a}{\mathrm{d}t}|\hat{a},\widehat{L};x,t\right\rangle = 0 \quad \text{and} \tag{42}$$

$$\left\langle \frac{\mathrm{d}L}{\mathrm{d}t}|\hat{a},\widehat{L};x,t\right\rangle = -\omega_{\hat{a}}\left(\widehat{L} - \overline{L}_{\hat{a}}\right) - \frac{1}{f}\frac{\partial(\sigma_{\hat{a}}^2\omega_{\hat{a}}f)}{\partial\widehat{L}} \tag{43}$$

in the x-,$\hat{a}$- and $\widehat{L}$-directions and therefore the modeled JPDF equation becomes

$$\frac{\partial f}{\partial t} + \frac{\partial}{\partial x}\left\{\frac{\widehat{L}f}{S_1\langle L|\hat{a}=1\rangle + S_2\langle L|\hat{a}=2\rangle}\right\} - \frac{\partial}{\partial\widehat{L}}\left\{\omega_{\hat{a}}(\widehat{L} - \overline{L}_{\hat{a}})f\right\} - \frac{\partial^2(\sigma_{\hat{a}}^2\omega_{\hat{a}}f)}{\partial\widehat{L}^2} = 0. \tag{44}$$

This is a Fokker–Planck equation, where the first term describes the temporal change of the f, the second term its transport in physical space, and the third and fourth terms describe drift and diffusion in the $\widehat{L}$-space. Multiplying the JPDF Eq. (44) with $(2-\hat{a})$ and subsequent integration over the $\hat{a}$–$\widehat{L}$-space leads to the saturation transport equation

$$\frac{\partial S_\alpha}{\partial t} + \frac{\partial}{\partial x}\left\{\frac{S_\alpha\langle L|\hat{a}=\alpha\rangle}{S_1\langle L|\hat{a}=1\rangle + S_2\langle L|\hat{a}=2\rangle}\right\} = 0, \tag{45}$$

which is identical with (37) for $\langle L|\hat{a}=\alpha\rangle = S_\alpha$ showing consistency with the equilibrium model. Similarly we can derive a transport equation for $S_\alpha\langle L|\hat{a}=\alpha\rangle$ by multiplying Eq. (44) with $\widehat{L}(2-\hat{a})$. Integration over the whole sample space then leads to

$$\begin{aligned}\frac{\partial S_\alpha\langle L|\hat{a}=\alpha\rangle}{\partial t} &+ \frac{\partial}{\partial x}\left\{\frac{S_\alpha\langle L|\hat{a}=\alpha\rangle^2}{S_1\langle L|\hat{a}=1\rangle + S_2\langle L|\hat{a}=2\rangle}\right\} + \frac{\partial}{\partial x}\left\{\frac{S_\alpha\langle (L-\langle L|\hat{a}=\alpha\rangle)^2|\hat{a}=\alpha\rangle}{S_1\langle L|\hat{a}=1\rangle + S_2\langle L|\hat{a}=2\rangle}\right\} \\ &+ \omega_\alpha(\langle L|\hat{a}=\alpha\rangle - \overline{L}_\alpha) = 0.\end{aligned} \tag{46}$$

Note that the moment Eqs. (45) and (46) do not form a closed system, since in general the third term on the left-hand side of Eq. (46) is unknown. On the other hand, this closure problem is avoided by directly solving the JPDF Eqs. (44), e.g. with the SPM.

The example above simply demonstrates how the SPM can be employed to use statistical moments and correlation structures of phase particle velocities (i.e. $\overline{L}_\alpha$, σ_α^2 and ω_α) to predict consistent statistical macroscopic behavior. The full advantage of such a stochastic approach becomes apparent, for example, if non-equilibrium physics involving non-trivial PDFs is considered.

6.1. Numerical results

Here we present a few simulation results, based on the non-equilibrium model explained above. As already mentioned in the previous subsection, the aim is to demonstrate how such simple Lagrangian rules lead to the results distinctly different from the corresponding equilibrium Darcy solutions. Note that it is not intended to propose a new physical model, however. For the studies we consider the same one-dimensional test case as in Section 5.1. Initially, the computational domain is populated with phase 1 particles, which are in equilibrium, i.e. $a^* = 1$ and $L^* = S_1 = 1$. From the left boundary, phase 2 particles with $a^* = 2$ and $L^* = S_2 = 1$ enter the domain. The relaxation time (dimensionless) $\tau'_\alpha = 1/\omega'_\alpha = \tau'$ is the same for all particles and σ_α is set to zero everywhere. Note that this model leads to $L^* = S_1$ and $L^* = S_2$ for phase 1 and phase 2 particles, respectively, if

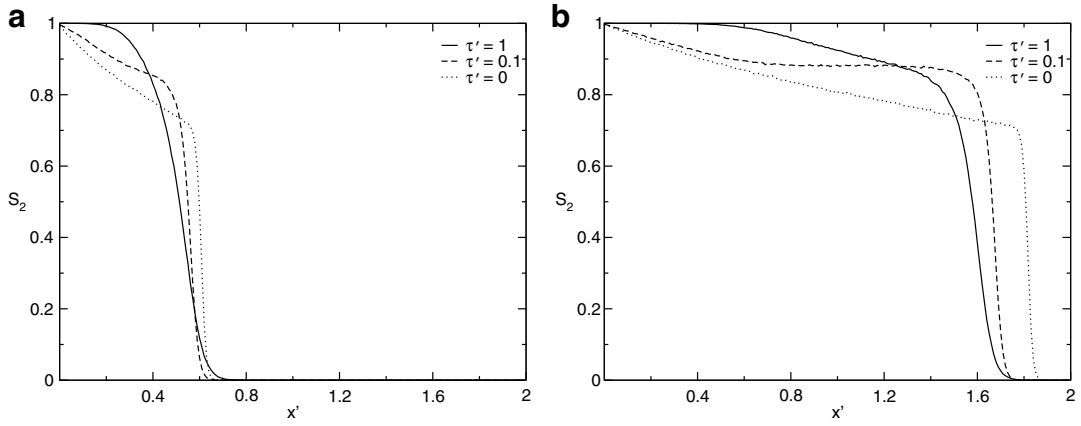

Fig. 12. Saturation evolution for different values of τ': (a) $t' = 0.5$; (b) $t' = 1.5$.

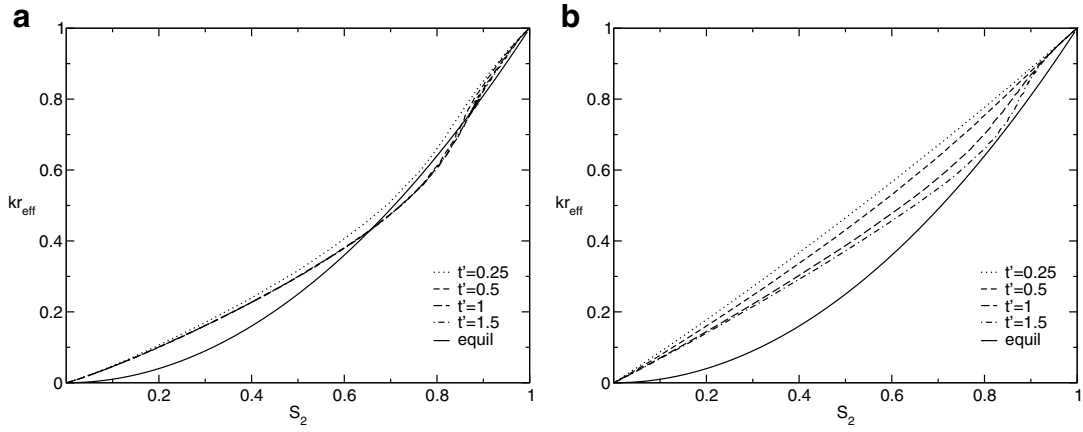

Fig. 13. The relative permeability curves as function of time: (a) $\tau' = 0.1$; (b) $\tau' = 1$.

$\tau' \to 0$. Otherwise, the distribution of L^* will be distinctly different; as the saturation profiles. For all simulations the viscosity ratio $M = 1$, the grid spacing $\Delta x' = 0.01$, $\mathrm{d}t' = 0.005$ and the average number of particles per cell was 50,000. Fig. 12 (a) and (b) depict the injected phase saturation profiles at two different times for $\tau' = 0$, $\tau' = 0.1$ and $\tau' = 1$. A significant departure from equilibrium can be observed. Figs. 13 (a) and (b) depict the effective relative permeability, $kr_{\mathrm{eff}} = S_2\langle L|\hat{a} = 2\rangle$, curves as function of injected phase saturation at four different times. One can observe that at late times the relative permeability curves approach a self-similar profile, which is different from the equilibrium curve and depends on τ'.

7. Discussion

The numerical examples and comparisons of Section 5 demonstrate that the SPM with appropriate rules for the phase particle movement is consistent with standard two-phase Darcy flow. In Section 6, it is shown how non-equilibrium effects can be modelled in the SPM framework. It has to be emphasized, however, that these studies only serve as a proof of concept for the SPM and demonstrate the power of SPM in modeling complex non-equilibrium phenomena. Below, the implications for physical modeling, but also the numerical difficulties and challenges are further discussed.

7.1. Implications for physical modeling

The motivation for the development of such a SPM is a computational framework, in which the histories of individual (infinitesimal) fluid volumes can be modeled depending on their phase, composition and other properties. It is important to distinguish between the SPM and deterministic particle methods such as characteristic methods or smooth particle hydrodynamics, where the particles carry saturation values. A particle in the SPM represents a fluid phase and moves with the phase particle velocity as opposed to the characteristic based method, where a particle moves with the characteristic velocity. As in the physical world, saturation is represented as a local, spatial average of phase volume ratios, i.e. saturation is a statistical quantity and not a particle property. Algorithmically, the saturation is estimated with local support (e.g. for the studies presented in this paper as cell averages). We expect that various complex physical processes can be described more directly and naturally than in a pure Eulerian framework, in which not individual fluid particle histories, but the evolution of mean values (e.g. saturations) at fix locations is modeled. For example, as shown in Section 6, evolution of a fluid particle, which depends on its history (and has memory) leads to non-equilibrium effects. These play a crucial role for trapping, dissolution and reaction processes and the SPM offers an alternative approach to model them. Moreover, although the SPM is not a pore scale model, it can provide a consistent link between the physics in the pores and the dynamics observed at Darcy scale. Therefore, however, the Lagrangian statistics of fluid particles has to be provided, e.g. from pore scale modeling. Note also that the particle ensemble represents the joint probability density function (PDF) of the particle properties (and not only first and maybe second moments) as a function of space and time. Similar PDF methods have been applied with considerable success to model turbulent reactive flows [26]. There, they have the significant advantages that turbulent convection and chemical reactions appear in closed form. Moreover, the huge amount of statistical information contained in the joint PDFs allows to develop more sophisticated models. On the other hand it has to be emphasized that a SPM simulation requires significantly more computer resources than a FVM study of the same test case. Therefore, we do not intend to use the SPM for very large studies, but rather to investigate how the macroscopic (Darcy scale) behavior relates to the physics and dynamics at the pore scale. We hope that such insight will ultimately lead to improved models for FVM simulators.

7.2. Numerical difficulties and challenges

As mentioned above, the SPM is computationally much more expensive than e.g. a FVM. This is due to the large number of particles, which is required to keep the statistical and the deterministic bias errors small. For example, the simulations discussed in this paper employed 10,000–50,000 particles per grid cell. Unfortunately, the statistical error $\varepsilon_{\mathrm{stat}}$ converges very slowly, i.e. $\varepsilon_{\mathrm{stat}} \sim 1/\sqrt{n}$, where n is the number of particles. Fig. 14 depicts the effect of n on the saturation profile. It is clear from the figure that even with few particles the expec-

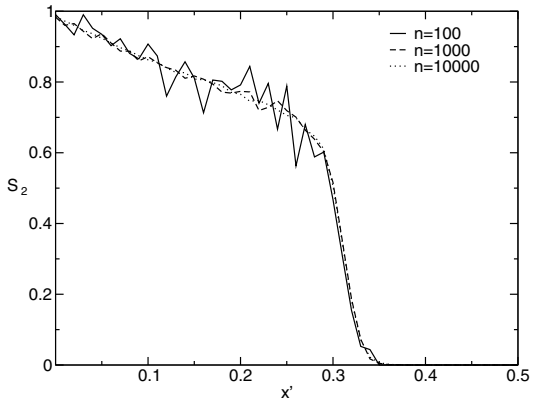

Fig. 14. The effect of number of computational particles used in the SPM simulation. Here n is the average number of particles per cell during the simulation.

tation of the solution is essentially the same, with a large statistical error, however. To reduce the statistical error without using too much memory, one can sample the results at several independent simulations (using different random number generator seeds) and then average the individual results in a postprocessing step. Note that the individual simulations can be done in parallel on standalone machines, i.e. no parallel computer is required. However, this approach does not help to reduce the deterministic bias error $\varepsilon_{\text{bias}}$ [30]. In order to control $\varepsilon_{\text{bias}}$, it is important to pay attention that the number of particles per cell is sufficiently high. Another issue, which is related to the required particle number, is the estimation of statistical moments from the particle field. For example, to resolve sharp fronts, a high spatial resolution is required. If the box method (sampling over grid cells) is employed, this implies that a finer grid and therefore in total more particles are required. The box method is only of first order spatial accuracy and it is similar to the first order finite volume method. It is worthwhile to investigate more sophisticated techniques to estimate saturation locally at particle locations. Possible alternatives might be based on spectral or wavelet methods [31]. In any case, however, one has to ensure that the dispersion in SPM simulations is dominated by the physical model and not by numerical errors.

8. Conclusions

In this paper, a stochastic particle method (SPM) to model nonlinear transport in porous media flow is presented. The motivation is the development of a modeling framework, in which the evolution of individual (infinitesimal) fluid volumes (particles) can be modeled directly depending on their phase, composition, and other properties. We believe that for various complex physical processes such a Lagrangian modeling approach is very natural and certainly provides an alternative viewpoint. The goal of the present work was to develop the basic SPM solution algorithm and to demonstrate that it is consistent with standard two phase Darcy flow, if appropriate rules for the particle evolution are employed. Therefore, various one- and two-dimensional validation studies were performed, which show that the SPM results converge to the expected solutions. The numerical algorithm requires a minimum amount of dispersion, i.e. pure shocks cannot be computed accurately. The amount of dispersion needed depends on the scheme used to estimate statistical moments, which may be improved in the future. Furthermore, with a simple illustrative example it is shown how the SPM can be used to model non-equilibrium transport effects. As a next step, it is planned to demonstrate that the SPM provides an alternative and attractive approach to model some of the complex phenomena, which are relevant for CO_2 storage and which have their origin at the pore scales.

Acknowledgments

The authors wish to acknowledge Dr. Benjamin Rembold with whom they had many useful discussions on technical issues during the development of the SPM C++ code. This research was supported by the Global Climate and Energy Project at Stanford University, USA.

Appendix

Here we provide the generalized fractional flow formulation for n-phases with capillary pressure differences. The phase fluxes according to Darcy's law reads

$$\boldsymbol{F}_i = -\frac{kr_i k}{\mu_i}\nabla p_i, \quad i \in \{1,\ldots,n\}, \tag{47}$$

Suppose we know $n-1$ independent relations between the pairs of pressures

$$p_{i-1} - p_i = p_{ci-1}, \quad i \in \{2,\ldots,n\}, \tag{48}$$

which are $n-1$ linear equations for n unknowns. Fixing the pressure of phase 1, p_1, and solving for the pressures of the rest of the phases yields

$$p_i = p_1 - \sum_{j=1}^{i-1} p_{cj}, \quad i \in \{2,\ldots,n\}. \tag{49}$$

Substituting Eq. (49) for p_i in Eq. (47) leads to

$$\boldsymbol{F}_i = -\frac{kr_i k}{\mu_i}\nabla\left(p_1 - \sum_{j=1}^{i-1} p_{cj}\right) = -\frac{kr_i k}{\mu_i}\nabla p_1 + \frac{kr_i k}{\mu_i}\sum_{j=1}^{i-1}\nabla p_{cj}, \quad i \in \{1,\ldots,n\}, \tag{50}$$

The total flux is obtained by summing up all the individual phase fluxes

$$\boldsymbol{F} = \sum_{l=1}^{n}\boldsymbol{F}_l = -k\sum_{l=1}^{n}\frac{kr_l}{\mu_l}\nabla p_l = -k\sum_{l=1}^{n}\frac{kr_l}{\mu_l}\nabla p_1 + k\sum_{l=1}^{n}\left(\frac{kr_l}{\mu_l}\sum_{j=1}^{l-1}\nabla p_{cj}\right) \tag{51}$$

from which follows that

$$-\nabla p_1 = \frac{\boldsymbol{F} - k\sum_{l=1}^{n}\left(\frac{kr_l}{\mu_l}\sum_{j=1}^{i-1}\nabla p_{cj}\right)}{k\sum_{l=1}^{n}\frac{kr_l}{\mu_l}}. \tag{52}$$

Substituting Eq. (52) for $-\nabla p_1$ in Eq. (50) results in the fractional flow formulation of Darcy's law, i.e.

$$\boldsymbol{F}_i = \frac{kr_i}{\mu_i}\frac{\left(\boldsymbol{F} - k\sum_{l=1}^{n}\left(\frac{kr_l}{\mu_l}\sum_{j=1}^{l-1}\nabla p_{cj}\right)\right)}{\sum_{l=1}^{n}\frac{kr_l}{\mu_l}} + \frac{kr_i k}{\mu_i}\sum_{j=1}^{i-1}\nabla p_{cj}, \quad i \in \{1,\ldots,n\} \tag{53}$$

or

$$\boldsymbol{F}_i = \frac{kr_i/\mu_i}{\sum_{l=1}^{n} kr_l/\mu_l}\boldsymbol{F} + \frac{-(kr_i k/\mu_i)\sum_{l=1}^{n}((kr_l/\mu_l)\sum_{j=1}^{l-1}\nabla p_{cj}) + (kr_i k/\mu_i)\sum_{l=1}^{n}(kr_l/\mu_l)\sum_{j=1}^{i-1}\nabla p_{cj}}{\sum_{l=1}^{n} kr_l/\mu_l}, \quad i \in \{1,\ldots,n\}. \tag{54}$$

The Poisson equation can be derived from the conservation law

$$\nabla\cdot\boldsymbol{F} = q \tag{55}$$

by substituting for $\boldsymbol{F}$ from Eq. (51) leads to

$$-\nabla\cdot\left(k\sum_{l=1}^{n}\frac{kr_l}{\mu_l}\nabla p_1\right) + \nabla\cdot\left(k\sum_{l=1}^{n}\left(\frac{kr_l}{\mu_l}\sum_{j=1}^{l-1}\nabla p_{cj}\right)\right) = q. \tag{56}$$

References

[1] M. Muskat, Physical Principles of Oil Production, McGraw-Hill, London, 1949.
[2] M. Blunt, M.J. King, H. Scher, Simulation and theory of 2-phase flow in porous media, Physical Review A 46 (1992) 7680–7699.
[3] R. Lenormand, E. Touboul, C. Zarcone, Numerical-models and experiments on immiscible displacement in porous-media, Journal of Fluid Mechanics 189 (1988) 165–187.

[4] R. Hilfer, P.E. Oren, Dimensional analysis of pore scale and field scale immiscible displacement, Transport in Porous Media 22 (1996) 53–72.
[5] S.W. Ahlstrom, H.P. Foote, R.C. Arnett, C.R. Cole, R.J. Serne, Multi-component mass transport model: theory and numerical implementation, Report. BNWL-2127, 1977.
[6] T.A. Prickett, T.G. Naymik, C.G. Longquist, A random walk solute transport model for selected groundwater quality evaluations, Report. I-11, 1981.
[7] W. Kinzelbach, Numerische Methoden zur Modellierung des Transports von Schadstoffen im Grundwasser, Oldenbourg Verlag, 1992.
[8] A.F.B. Tompson, L.W. Gelhar, Numerical simulation of solute transport in three-dimensional, randomly heterogenous porous media, Advances in Water Resources 26 (1990) 2541–2562.
[9] D. Zhang, L. Li, H.A. Tchelepi, Stochastic formulation for uncertainty analysis of two-phase flow in heterogeneous reservoirs, SPE Journal 5 (2000) 60–70.
[10] D.W. Pollock, Semianalytical computation of path lines for finite difference models, Groundwater 26 (1988) 743–750.
[11] D.J. Goode, Particle velocity interpolation in block-centered finite difference groundwater flow models, Water Resources Research 26 (1990) 925–940.
[12] M.A. Celia, T.F. Russell, I. Herera, R.E. Ewing, An Eulerian–Lagrangian localized adjoint method for the advection–diffusion equation, Advances in Water Resources 13 (1990) 187–206.
[13] L.F. Konikov, D.J. Goode, G.Z. Hornberger, A three-dimensional method of characteristics solute transport model (moc3d), Water Resources Investigation Report 96–4267, 1996.
[14] T.F. Russel, M.A. Celia, An overview of research on Eulerian–Lagrangian localized adjoint methods (ELLAM), Advances in Water Resources 25 (2002) 1215–1231.
[15] H.K. Dahle, M.S. Espendal, R.E. Ewing, O. Sævaried, Characteristic adaptive subdomain methods for reservoir flow problems, Numerical Methods for Partial Differential Equations 6 (1990) 279–309.
[16] H.K. Dahle, R.E. Ewing, T.F. Russell, Eulerian–Lagrangian localized adjoint methods for a nonlinear advection–diffusion equation, Computer Methods in Applied Mechanics and Engineering 122 (1995) 223–250.
[17] T.A. Hewett, T. Yamada, Theory for the semi-analytic calculation of oil recovery and effective relative permeabilities using streamtubes, Advances in Water Resources 20 (1997) 279–292.
[18] J. Herzer, W. Kizelbach, Coupling of transport and chemical processes in numerical transport models, Geoderma 44 (1989) 115–127.
[19] A. Abulaban, J.L. Nieber, D. Misra, Modeling plume behavior for nonlinearly sorbing solutes in saturated homogeneous porous media, Advances in Water Resources 21 (1998) 487–498.
[20] F. Delay, Ph. Ackerer, C. Danquigny, Simulating solute transport in porous media or fractured formations using random walk particle tracking: a review, Vadose Zone Journal 4 (2005) 360–379.
[21] A.C. Bagtzoglou, A.F.B. Tompson, D.E. Dougherty, Projection functions for particle-grid methods, Numerical Methods for Partial Differential Equations 8 (1992) 325–340.
[22] M.R. Thiele, R.P. Batycky, M.J. Blunt, A streamline-based field-scale compositional reservoir simulator, in: SPE Annual Technical Conference and Exhibition, San Antonio, TX, October 5–8, 1997, SPE 38889.
[23] G. Dagan, V. Cvetkovic, Reactive transport and immiscible flow in geological media. I. General theory, Proceeding of Royal Society London A 452 (1996) 285–301.
[24] V. Cvetkovic, G. Dagan, Reactive transport and immiscible flow in geological media. II. Applications, Proceeding of Royal Society London A 452 (1996) 303–328.
[25] M.R. Thiele, H.A. Tchelepi, F.M. Orr, On particle tracking in multi-phase, multi-component flow, Unpublished work, 1992.
[26] S.B. Pope, Pdf methods for turbulent reactive flows, Progress in Energy and Combustion Science 11 (1985) 119–192.
[27] P.E. Kloeden, E. Platen, Numerical Solution of Stochastic Differential Equations, Springer, 1999.
[28] B. Rembold, P. Jenny, A multiblock joint PDF finite-volume hybrid algorithm for the computation of turbulent flows in complex geometries, Journal of Computational Physics 220 (2006) 59–87.
[29] B.P. Leonard, A stable and accurate convective modeling procedure based on quadratic upstream interpolation, Computer Methods in Applied Mechanics and Engineering 19 (1979) 59–98.
[30] J. Xu, S.B. Pope, Assessment of numerical accuracy of PDF/Monte Carlo methods for turbulent reacting flows, Journal of Computational Physics 152 (1999) 192–230.
[31] Q. Zhang, K. Ichiki, A. Prosperetti, On the computation of ensemble of average for spatially non-uniform particle system, Journal of Computational Physics 212 (2006) 247–267.